Journal of Sound and Vibration 490 (2021) 115735

Contents lists available at ScienceDirect

Journal of Sound and Vibration

journal homepage: www.elsevier.com/locate/jsv

Extracting multiple bridge frequencies from test vehicle – a theoretical study

Zhenhua Shi*, Nasim Uddin

Department of Civil, Construction and Environmental Engineering, The University of Alabama at Birmingham, Birmingham, AL, 35294, USA

ARTICLE INFO

Article history:
Received 5 April 2020
Revised 15 August 2020
Accepted 21 September 2020
Available online 22 September 2020

Keywords:
Coupled differential equation
Damping
Vehicle bridge interaction
Structural dynamics

ABSTRACT

The coupled differential equation group for the vehicle bridge interaction system is reestablished to include both the vehicle and bridge damping effects. The equation group can be uncoupled and closed-form solutions for both the bridge and vehicle can be obtained under the assumption that the vehicle acceleration magnitude is much lower than the gravitational acceleration constant. Then based on a simply supported boundary condition scenario, several critical parameters including bridge damping, vehicle frequency, vehicle speed, vehicle mass, and vehicle damping are studied to investigate their effects on extracting multiple bridge frequencies from the vehicle. The results show that the bridge damping plays a significant role in the vibration behaviour of both the vehicle and the bridge compared to the vehicle damping. The vehicle is preferred to be designed with a high frequency beyond the interested bridge frequencies to be extracted since low vehicle frequency tends to attenuate bridge frequencies that are higher than the vehicle frequency. A camel hump phenomenon can be observed on the extracted bridge frequencies from the vehicle, especially for scenarios that involve high bridge vibration mode and high vehicle speed. Vehicle speed is preferred to be maintained low to meet the theoretical assumption and to reduce the camel hump phenomenon. Although vehicle mass is not necessarily limited in this study, there is a magnitude balance among vehicle mass, vehicle speed, and damping to meet the theoretical assumption. This theoretical work may give some indications for designing a special field test vehicle to monitor bridge in a more comprehensive way.

1. Introduction

Vehicle bridge interaction (VBI) is a fundamental issue for fully understanding the dynamic behaviour of both the vehicle and bridge during their interaction and has been widely studied both theoretically and experimentally for decades. Theoretically understanding of the interaction has the potential significance not only for designing the bridges but also that the dynamic characteristics of one can be derived by the other. For instance, on one hand, the vehicle weight can be estimated based on the bridge response to monitor and potentially regulate vehicles that may have excessive loads in the transportation network [1–4]. On the other hand, the vehicle-based structural health monitoring (SHM) of bridges has also been gained wide attention due to the advantages of mobility and potential economy characteristics [5,6]. The intention

* Corresponding author.
E-mail addresses: zhs@uab.edu (Z. Shi), nuddin@uab.edu (N. Uddin).

https://doi.org/10.1016/j.jsv.2020.115735
0022-460X/

behind this approach is that the bridge dynamic information such as frequencies [7–16], mode shapes [17–22], and damping properties [23,24] can be interpreted by the dynamic response of the passing vehicle. The readers may be directed to a complete review of VBI related theory and application by Yang et al. [25] about vehicle scanning method for bridges.

Back in 2004, Yang et al. [7] established a theoretical VBI model without both the vehicle and bridge damping effects to extract bridge fundamental frequency from the dynamic response of a passing vehicle. Under the assumption that the vehicle has a mass that is an order magnitude lower than the total bridge mass, the closed-form solutions were obtained considering only the first mode of the bridge. Only the first bridge frequency could be detected from the vehicle since only the first bridge vibration mode was considered in the equations. Based on this theoretical VBI model, Yang et al. [17,22] further constructed the mode shapes of the bridge using the dynamic response of the passing vehicle, under the assumption that the driving frequency is much lower than the bridge frequency. However, Yang and Lee [13] pointed out that vehicle damping is one of the key factors that affect the extraction of bridge frequency results. Their numerical studies show that high vehicle damping is beneficial to suppress the road surface roughness as well as the vehicle frequency. Nevertheless, only the first bridge frequency was studied. Yang and Cao recently [14] proposed a double-mass vehicle model of VBI system to include the wheel size effect, in which the vehicle was modelled as a sprung mass representing the vehicle body and an un-sprung disk representing the axle mass with the wheel radius. The damping for the suspension system was considered in their model but not for the wheel since the commercial wheel usually consists of a rigid alloy rim and a pneumatic tire. The pneumatic tire, which is designed to provide a contact patch cushion, or “footprint”, to absorb shock and to avoid excessive bearing pressure, is believed to have significant damping contribution. In other words, the rigid alloy rim was represented but not the pneumatic tire. Due to the complexity of the problem, the system was studied by finite element method rather than analytical explicit solutions or closed-form solutions. The merit of closed-form solutions is that it may directly reveal the frequency components of both the bridge and vehicle responses so that one would expect certain features during a realistic experiment. The theoretical studies reviewed here show that the mathematical model of the VBI system is still not well represented. A new mathematical model considering both the bridge and vehicle damping effects is proposed in this study, and the analytical explicit solutions are sought to reveal the frequency components of both the bridge and vehicle responses.

Besides theoretical study, numerous experimental studies were also conducted to verify or explore vehicle-based approach in field applications. In the following experimental verification study, Lin and Yang [9] used an accelerometer-installed cart towed by a truck to identify the fundamental bridge frequency. Their results show that the first bridge frequency can be identified if the vehicle is maintained at a proper low speed. However, even the second vertical bridge frequency (besides bridge lateral mode) was not identified in their field tests. A hand-drawn cart field study in 2013 [12] shows that the PU (polyurethane) wheels were the most suitable for extracting bridge frequencies compared to inflatable wheels and rubber wheels, their study shows that heavier cart with low speed could identify multiple bridge frequencies. Since the wheel size is relatively small compared to the bridge surface roughness, separation might occur which may void the analytical solutions. For commercial wheels with inflated tires, the contact patch may counterbalance the roughness of the asphalt so that separation is less likely to occur. Kim and Lynch [26] used wireless sensors deployed on a heavy vehicle and a continuous steel bridge to study a realistic field VBI scenario. The bridge frequencies were not identified from the heavy truck due to possible attenuation effect of the suspension system, while this study indicates that the reason could also be simply the low-frequency effect due to the inflated tires. In their level 1 screening experiment, Kim et al. [27] experimentally studied the feasibility of using the vehicle response to monitor a short span bridge, the damages of which were represented by dampers (old displacement transducers) and additional mass. They concluded that it is possible to detect bridge frequency changes due to structural damage under restricted conditions. However, only the first bridge frequency was investigated. The spectra may also be controversial since the vehicle frequency and first bridge frequency were close, especially considering the possible bridge frequency shift due to numerous side effects. Cerda et al. [28] experimentally studied the vehicle-based approach for detecting different scenarios including support rotation restrictions, additional damping, and additional mass, based on only the first bridge frequency identification results. McGetrick et al. [29] experimentally monitored the bridge stiffness using the vehicle response, while only the first frequency of the bridge can be identified. Urushadze and Yau [16] used a stiffness-adjustable vehicle to test the frequencies of a plexiglass beam, they concluded that vehicle with harder spring gave better predictions of the bridge frequencies. Kim et al. [30] used a tractor-trailer vehicle to detect the bridge frequency, in which only the first bridge frequency was identified with an error of 8.8%. The perennial problem of experimental observations as reviewed here is that only the first bridge frequency (sometimes none, in rare cases, the first two) could be identified and most of the results may still be controversial if one inspects various spectra carefully. This is far from monitoring the bridges in a comprehensive way. From structural dynamics point of view, the integrity of the structural dynamic characteristics of the bridge such as frequency, mode shape and damping ratio group list, should be relied on to comprehensively evaluate and monitor the bridge, rather than only the first frequency of the bridge. Therefore, this study is also trying to provide a theoretical reference for designing a special test vehicle so that more bridge dynamic information may be reflected.

To account for both the bridge and vehicle damping effect and to extract multiple bridge dynamic information, this study reestablishes the coupled equation group for the VBI system and presents several critical assumptions and discussions when extracting multiple frequencies information. The equation group features that it includes the damping effects for both the vehicle and bridge and is open for any other kinds of bridge boundary conditions. The equation group is uncoupled under a new assumption and closed-form solutions are obtained for the bridge with simply supported boundary condition scenario,

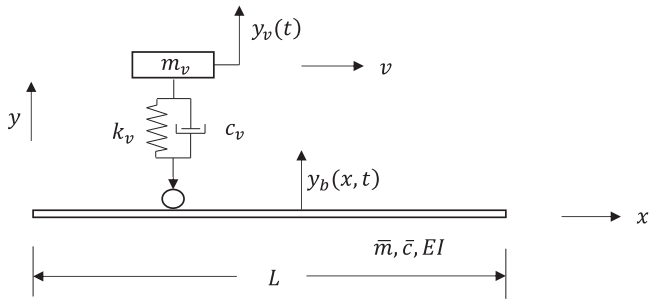

Fig. 1. General VBI model without boundary conditions.

and critical vehicle design parameters including frequency, speed, mass, and damping are studied. It needs to be mentioned that the road surface roughness is not considered in this study. Firstly, the inclusion of bridge surface roughness into the equations would significantly complicate the problem and closed-form solutions may not be readily obtained. Secondly, the effect of road profile is believed to be dependent on the contact patch size. A large contact patch would significantly counterbalance the bridge profile to avoid separation, while a tiny contact patch may introduce separation and impact between the vehicle and the bridge which may require a much more complicated mathematical model. The theoretical expressions were implemented in MATLAB [31] to present the results in graphics. This study is organized as follows: theoretical formulation is introduced in Section 2; analytical study using baseline parameters is presented in Section 3; while parameter studies are presented in Sections 4 and 5, followed by conclusions in Section 6.

2. Theoretical formulation

2.1. Equation group for general VBI

A general VBI system without boundary conditions is illustrated in Fig. 1. The bridge is considered as a Bernoulli-Euler beam with uniformly distributed properties including unit-length mass constant $\bar{m}$, unit-length damping constant $\bar{c}$, and section stiffness EI, while the vehicle is simplified as a damped sprung mass with properties of mass m_v, spring constant k_v, and damping constant c_v. A Bernoulli-Euler beam assumes that a plane cross-section remains a plane during flexure. For the vehicle, the problem is essentially to determine the response of the damped sprung mass due to the support motion. By ignoring the flexure effects caused by shear, rotary inertial, and axial forces, the equilibrium equation of the VBI system can be established as

$$\begin{cases} m_v\ddot{y}_v + c_v(\dot{y}_v - \dot{y}_b|_{x=vt}) + k_v(y_v - y_b|_{x=vt}) = 0 \\ \bar{m}\frac{\partial^2 y_b}{\partial t^2} + \bar{c}\frac{\partial y_b}{\partial t} + EI\frac{\partial^4 y_b}{\partial x^4} = p(x,t) \end{cases} \tag{1}$$

in which y_v is the vehicle displacement which is a function of time, y_b is the bridge displacement which is a function of both time and space, head dots are used for derivatives with respect to time, the partial differential symbol ∂ is used for functions that have two or more variables. The lateral load distribution $p(x, t)$, is zero everywhere along the bridge except for a concentrated load at the contact point between the vehicle and the bridge. $p(x, t)$ can be described as

$$p(x,t) = \begin{cases} k_v(y_v - y_b|_{x=vt}) + c_v(\dot{y}_v - \dot{y}_b|_{x=vt}) - m_v g \\ 0 \end{cases} = \begin{cases} -m_v\ddot{y}_v - m_v g, & x = vt \\ 0, & x \neq vt \end{cases} \tag{2}$$

the coupled equilibrium equation group of the VBI system will then be

$$\begin{cases} m_v\ddot{y}_v + c_v\dot{y}_v + k_v y_v = k_v y_b|_{x=vt} + c_v\dot{y}_b|_{x=vt} \\ \bar{m}\frac{\partial^2 y_b}{\partial t^2} + \bar{c}\frac{\partial y_b}{\partial t} + EI\frac{\partial^4 y_b}{\partial x^4} = \begin{cases} -m_v(\ddot{y}_v + g), & x = vt \\ 0, & x \neq vt \end{cases} \end{cases} \tag{3}$$

The orthogonal nature of normal modes provides a way to address a system that has multiple degree-of-freedom by superposition, in which the vibration of the system can be expressed in terms of the superposition of normal modes [32]. Thus, the solution of the bridge equation can be found by the method of separation of variables, in which the solution is assumed as an infinite superposition of the product of the normal modes $\Phi_n(x)$ and time functions $z_n(t)$ in the following form

$$y_b(x,t) = \sum_n \Phi_n(x) z_n(t) \tag{4}$$

substituting into the equation group would result in

$$\begin{cases} m_v\ddot{y}_v + c_v\dot{y}_v + k_v y_v = \sum_n [k_v z_n(t) + c_v \dot{z}_n(t)]\Phi_n(vt) \\ \ddot{z}_n(t) + \frac{\bar{c}}{\bar{m}}\dot{z}_n(t) + \omega_n^2 z_n(t) = \frac{\int_0^L \Phi_n(x)\begin{cases} -m_v(\ddot{y}_v + g), & x = vt \\ 0, & x \neq vt \end{cases} dx}{\bar{m}\int_0^L \Phi_n^2(x)dx} \end{cases} \tag{5}$$

in which $\bar{c}$ and $\bar{m}$ are assumed as constants; while $\Phi_n(x)$ and ω_n depend on the bridge boundary conditions and have the following relationship

$$\Phi_n^{IV}(x) - \frac{\bar{m}\omega_n^2}{EI}\Phi_n(x) = 0 \tag{6}$$

here the roman indices indicate derivatives with respect to the space variable x. The coupled differential equation group Eq. (5) that contains the variable of $z_n(t)$ and $y_v(t)$, is the exact equation group to be solved for the VBI system with both the vehicle and bridge damping effect for any bridge boundary conditions.

2.2. Bridge response

Although the VBI equation group in Section 2.1 is open for bridges with any boundary conditions, the normal mode expressions may be complicated except for the simply supported scenario. To have some practical implications for field application and to present basic steps adopted to address the VBI system, the equation group is uncoupled and solved for the bridge with simply supported boundary condition, bridges with other types of boundary conditions may be studied in future research. For simply supported boundary condition, the normal modes are

$$\Phi_n = \sin\frac{n\pi x}{L} \tag{7}$$

the corresponding natural frequencies are

$$\omega_n = n^2\pi^2\sqrt{\frac{EI}{\bar{m}L^4}} \tag{8}$$

the equation group Eq. (5) can be uncoupled if assuming $\ddot{y}_v \ll g$, in which case the equation of the bridge will be

$$\ddot{z}_n(t) + \frac{\bar{c}}{\bar{m}}\dot{z}_n(t) + \omega_n^2 z_n(t) = -\frac{2m_v g}{\bar{m}L}\sin\frac{n\pi vt}{L} \tag{9}$$

the solution to this second-order ordinary differential equation is

$$\begin{aligned} z_n(t) = {} & e^{-\xi_n\omega_n t}\left[A_n\cos\left(\sqrt{1-\xi_n^2}\right)\omega_n t + B_n\sin\left(\sqrt{1-\xi_n^2}\right)\omega_n t\right] \\ & - \frac{2m_v g}{\bar{m}L\omega_n^2\sqrt{\left(1-r_n^2\right)^2 + \left(2r_n\xi_n\right)^2}}\sin\left(\frac{n\pi v}{L}t - \theta_n\right) \end{aligned} \tag{10}$$

in which,

$$\xi_n = \frac{\bar{c}}{2\bar{m}\omega_n}, \tag{11}$$

$$r_n = \frac{n\pi v}{\omega_n L}, \tag{12}$$

$$\tan\theta_n = \frac{2r_n\xi_n}{1-r_n^2} \tag{13}$$

for zero initial conditions (bridge in the static equilibrium state), that is $z_n(0) = 0$, and $\dot{z}_n(0) = 0$, A_n and B_n can be calculated as

$$\begin{cases} A_n = -\frac{4m_v g r_n\xi_n}{\bar{m}L\omega_n^2\left[\left(1-r_n^2\right)^2 + \left(2r_n\xi_n\right)^2\right]} \\ B_n = \frac{2m_v g\left[\left(1-r_n^2\right)\frac{n\pi v}{L} - 2\xi_n\omega_n r_n\xi_n\right]}{\bar{m}L\omega_n^2\left[\left(1-r_n^2\right)^2 + \left(2r_n\xi_n\right)^2\right]\left(\sqrt{1-\xi_n^2}\right)\omega_n} \end{cases} \tag{14}$$

once obtaining the time function, the displacement and acceleration response of the bridge can be respectively obtained as

$$y_b(x,t) = \sum_n \left\{ \begin{aligned} & e^{-\xi_n\omega_n t}\left[A_n\cos\left(\sqrt{1-\xi_n^2}\right)\omega_n t + B_n\sin\left(\sqrt{1-\xi_n^2}\right)\omega_n t\right] \\ & - \frac{2m_v g}{\bar{m}L\omega_n^2\sqrt{\left(1-r_n^2\right)^2 + \left(2r_n\xi_n\right)^2}}\sin\left(\frac{n\pi v}{L}t - \theta_n\right) \end{aligned} \right\} \sin\frac{n\pi x}{L} \tag{15}$$

$$\ddot{y}_b(x,t)=\sum_n\left\{\begin{array}{l}e^{-\xi_n\omega_n t}\left\{\begin{array}{c}\left[\begin{array}{c}(\xi_n\omega_n)^2A_n-2\xi_n\left(\sqrt{1-\xi_n^2}\right)\omega_n^2B_n\\-\left(1-\xi_n^2\right)\omega_n^2A_n\end{array}\right]\cos\left(\sqrt{1-\xi_n^2}\right)\omega_n t\\+\left[\begin{array}{c}(\xi_n\omega_n)^2B_n+2\xi_n\left(\sqrt{1-\xi_n^2}\right)\omega_n^2A_n\\-\left(1-\xi_n^2\right)\omega_n^2B_n\end{array}\right]\sin\left(\sqrt{1-\xi_n^2}\right)\omega_n t\end{array}\right\}\\+\frac{2m_v g}{\bar{m}L\omega_n^2\sqrt{\left(1-r_n^2\right)^2+\left(2r_n\xi_n\right)^2}}\left(\frac{n\pi v}{L}\right)^2\sin\left(\frac{n\pi v}{L}t-\theta_n\right)\end{array}\right\}\sin\frac{n\pi x}{L}\tag{16}$$

It can be seen that the bridge responses are dominated by two different categories of frequency: damped bridge frequencies $(\sqrt{1-\xi_n^2})\omega_n$ and vehicle driving frequency $\frac{n\pi v}{L}$. Those two different categories of frequency may all be expected from the bridge signal. The instantaneous vehicle load can also be thought as a superposition of sequential time-varying impulse loads (coupled with the bridge response, rather than a known load with an expression) applied to the bridge, and since these loads include both symmetrical and antisymmetric scenarios, all the normal modes should be excited on the bridge. The implication here is that all the bridge frequency information could be transmitted to and then extracted from the test vehicle. Besides, the damping effect may not be neglected since new impulse loads are introduced constantly to the bridge so long as the vehicle is still travelling on the bridge. Inclusion of the damping effects also provides a theoretical reference not only to the structural interaction that involves significant damping properties, but also to the discrepancies between theoretical studies and experimental observations, as shown in the analytical study Section 3, both the bridge and vehicle responses will be quite different when the damping effect is considered.

2.3. Vehicle response

To extract the dynamic information of the bridge from the vehicle signal, the vehicle responses need also to be determined. Once obtaining the time function $z_n(t)$ of the bridge, the equation for the vehicle becomes

$$\ddot{y}_v+2\xi_v\omega_v\dot{y}_v+\omega_v^2y_v=\sum_n\left\{\begin{array}{c}e^{-\xi_n\omega_n t}\left\{\begin{array}{l}E_n\cos\left[\left(\sqrt{1-\xi_n^2}\right)\omega_n t\right]\\+F_n sin\left[\left(\sqrt{1-\xi_n^2}\right)\omega_n t\right]\end{array}\right\}\\-\omega_v^2D_n\sin\left(\frac{n\pi v}{L}t-\theta_n\right)\\-2\xi_v\omega_vD_n\frac{n\pi v}{L}\cos\left(\frac{n\pi v}{L}t-\theta_n\right)\end{array}\right\}\sin\frac{n\pi vt}{L}\tag{17}$$

in which

$$\left\{\begin{array}{l}E_n=\omega_v^2A_n-2\xi_v\omega_vA_n\xi_n\omega_n+2\xi_v\omega_vB_n\left(\sqrt{1-\xi_n^2}\right)\omega_n\\F_n=\omega_v^2B_n-2\xi_v\omega_vB_n\xi_n\omega_n-2\xi_v\omega_vA_n\left(\sqrt{1-\xi_n^2}\right)\omega_n\\D_n=\frac{2m_v g}{\bar{m}L\omega_n^2\sqrt{\left(1-r_n^2\right)^2+\left(2r_n\xi_n\right)^2}}\end{array}\right.\tag{18}$$

the equation of the vehicle needs to be further deduced to incorporate the time-variant term $\sin\frac{n\pi vt}{L}$ which is located outside of the curly brackets. The equation becomes

$$\ddot{y}_v+2\xi_v\omega_v\dot{y}_v+\omega_v^2y_v=\sum_n\left(\begin{array}{l}\frac{E_n}{2}e^{-\xi_n\omega_n t}\sin\bar{\omega}_{n+}t+\frac{E_n}{2}e^{-\xi_n\omega_n t}\sin\bar{\omega}_{n-}t\\+\frac{F_n}{2}e^{-\xi_n\omega_n t}\cos\bar{\omega}_{n-}t-\frac{F_n}{2}e^{-\xi_n\omega_n t}\cos\bar{\omega}_{n+}t\\-\frac{D_nP_n}{2}+\frac{D_nP_n}{2}\cos\frac{2n\pi v}{L}t+\frac{D_nQ_n}{2}\sin\frac{2n\pi v}{L}t\end{array}\right)\tag{19}$$

in which

$$\left\{\begin{array}{l}\bar{\omega}_{n\pm}=\frac{n\pi v}{L}\pm\left(\sqrt{1-\xi_n^2}\right)\omega_n\\P_n=\omega_v^2\cos\theta_n+2\xi_v\omega_v\frac{n\pi v}{L}\sin\theta_n\\Q_n=\omega_v^2\sin\theta_n-2\xi_v\omega_v\frac{n\pi v}{L}\cos\theta_n\end{array}\right.\tag{20}$$

the solution to the differential Eq. (19) can be obtained by solving each right-hand term and then superposing them together. Theoretically, the total response of the vehicle will then be the superposition of an infinite number of bridge vibration modes. The displacement and acceleration response of the vehicle can be deduced respectively as:

$$y_v(t)=\sum_n\left\{\begin{array}{l}e^{-\xi_v\omega_v t}\left[A_n^*\cos\left(\sqrt{1-\xi_v^2}\right)\omega_v t+B_n^*\sin\left(\sqrt{1-\xi_v^2}\right)\omega_v t\right]\\+e^{-\xi_n\omega_n t}\left(C_{1n}^*\sin\bar{\omega}_{n+}t+C_{2n}^*\sin\bar{\omega}_{n-}t+C_{3n}^*\cos\bar{\omega}_{n+}t+C_{4n}^*cos\bar{\omega}_{n-}t\right)\\-\frac{D_nP_n}{2\omega_v^2}+\frac{D_n}{2\omega_v^2}\frac{1}{\left(1-r_v^2\right)^2+\left(2r_v\xi_v\right)^2}\left\{\begin{array}{l}\left[2r_v\xi_vP_n+\left(1-r_v^2\right)Q_n\right]\sin\frac{2n\pi v}{L}t\\+\left[\left(1-r_v^2\right)P_n-2r_v\xi_vQ_n\right]\cos\frac{2n\pi v}{L}t\end{array}\right\}\end{array}\right\}\tag{21}$$

$$\ddot{y}_v(t)=\sum_n\left\{\begin{array}{l} e^{-\xi_v\omega_v t}\left\{\begin{array}{l}\left[A_n^*(\xi_v\omega_v)^2-2B_n^*\xi_v\left(\sqrt{1-\xi_v^2}\right)\omega_v^2-A_n^*\left(1-\xi_v^2\right)\omega_v^2\right]\cos\left(\sqrt{1-\xi_v^2}\right)\omega_v t\\ +\left[B_n^*(\xi_v\omega_v)^2+2A_n^*\xi_v\left(\sqrt{1-\xi_v^2}\right)\omega_v^2-B_n^*\left(1-\xi_v^2\right)\omega_v^2\right]\sin\left(\sqrt{1-\xi_v^2}\right)\omega_v t\end{array}\right\}\\ +e^{-\xi_n\omega_n t}\left\{\begin{array}{l}\left[C_{1n}^*(\xi_n\omega_n)^2+2C_{3n}^*\xi_n\omega_n\bar{\omega}_{n+}-C_{1n}^*\bar{\omega}_{n+}^2\right]\sin\bar{\omega}_{n+}t\\ +\left[C_{2n}^*(\xi_n\omega_n)^2+2C_{4n}^*\xi_n\omega_n\bar{\omega}_{n-}-C_{2n}^*\bar{\omega}_{n-}^2\right]\sin\bar{\omega}_{n-}t\\ +\left[C_{3n}^*(\xi_n\omega_n)^2-2C_{1n}^*\xi_n\omega_n\bar{\omega}_{n+}-C_{3n}^*\bar{\omega}_{n+}^2\right]\cos\bar{\omega}_{n+}t\\ +\left[C_{4n}^*(\xi_n\omega_n)^2-2C_{2n}^*\xi_n\omega_n\bar{\omega}_{n-}-C_{4n}^*\bar{\omega}_{n-}^2\right]\cos\bar{\omega}_{n-}t\end{array}\right\}\\ -\frac{D_n}{2\omega_v^2}\left(\frac{2n\pi v}{L}\right)^2\frac{1}{\left(1-r_v^2\right)^2+(2r_v\xi_v)^2}\left\{\begin{array}{l}\left[2P_n r_v\xi_v+\left(1-r_v^2\right)Q_n\right]\sin\frac{2n\pi v}{L}t\\ +\left[P_n\left(1-r_v^2\right)-2r_v\xi_v Q_n\right]\cos\frac{2n\pi v}{L}t\end{array}\right\}\end{array}\right\} \tag{22}$$

in which

$$r_v=\frac{2n\pi v}{\omega_v L}, \tag{23}$$

$$\tan\theta_v=\frac{2r_v\xi_v}{1-r_v^2} \tag{24}$$

$$\left\{\begin{array}{l}A_n^*=-\left(C_{3n}^*+C_{4n}^*\right)+\frac{D_n}{2\omega_v^2}\left\{P_n-\frac{P_n\left(1-r_v^2\right)-Q_n 2r_v\xi_v}{\left[\left(1-r_v^2\right)^2+(2r_v\xi_v)^2\right]}\right\}\\ B_n^*=\frac{\left(C_{3n}^*+C_{4n}^*\right)(\xi_n\omega_n-\xi_v\omega_v)-C_{1n}^*\bar{\omega}_{n+}-C_{2n}^*\bar{\omega}_{n-}}{\omega_v\sqrt{1-\xi_v^2}}+\frac{D_n}{2\omega_v^2\sqrt{1-\xi_v^2}}\left\{P_n\xi_v-\frac{P_n\xi_v\left(1+r_v^2\right)-Q_n r_v\left(2\xi_v^2+r_v^2-1\right)}{\left[\left(1-r_v^2\right)^2+(2r_v\xi_v)^2\right]}\right\}\end{array}\right. \tag{25}$$

$$\left\{\begin{array}{l}C_{1n}^*=\frac{E_n M_{n+}+F_n N_{n+}}{2\left(M_{n+}^2+N_{n+}^2\right)}\\ C_{2n}^*=\frac{E_n M_{n-}-F_n N_{n-}}{2\left(M_{n-}^2+N_{n-}^2\right)}\\ C_{3n}^*=\frac{E_n N_{n+}-F_n M_{n+}}{2\left(M_{n+}^2+N_{n+}^2\right)}\\ C_{4n}^*=\frac{E_n N_{n-}+F_n M_{n-}}{2\left(M_{n-}^2+N_{n-}^2\right)}\end{array}\right. \tag{26}$$

$$\left\{\begin{array}{l}M_{n\pm}=(\xi_n\omega_n)^2-\bar{\omega}_{n\pm}^2-2\xi_v\omega_v\xi_n\omega_n+\omega_v^2\\ N_{n\pm}=2\bar{\omega}_{n\pm}(\xi_n\omega_n-\xi_v\omega_v)\end{array}\right. \tag{27}$$

It can be seen that the vehicle responses are dominated by three different categories of frequency: the damped vehicle frequency $(\sqrt{1-\xi_v^2})\omega_v$, vehicle driving frequency affected damped bridge frequencies $\frac{n\pi v}{L}\pm(\sqrt{1-\xi_n^2})\omega_n$, and doubled vehicle driving frequency $\frac{2n\pi v}{L}$. The other two types of frequency components may need to be properly adjusted so that the interested multiple bridge frequencies are not disturbed and can be readily identified. It also needs to be pointed out that, when neglecting the damping effects by assuming $\xi_v=0$ and $\xi_n=0$, the solutions of the vehicle will be interestingly simplified to be left with only the cosine terms, which is also consistent with theoretical models from the literature [22], but the rationale behind the simplification of the initial coupled differential equation group is that the vehicle acceleration magnitude is negligible compared to g, rather than that the vehicle mass is far lower than the bridge mass. Analytical study sections show that not only the vehicle mass but also the vehicle speed will affect the vehicle acceleration magnitude, the indication here is that the travelling speed can be kept low for the heavy vehicle to meet the assumption. In a scenario study of the vehicle having a mass as high as 100% of the bridge, but with a travelling speed as 8.94 m·s^{-1} on a 30.48 m long bridge, the vehicle acceleration magnitude is only 2.26%g, which may still meet the theoretical assumption.

3. Analytical baseline study

A 100-ft (30.48 m) long bridge example [33] is adopted to illustrate the theoretical solutions obtained in Section 2. It needs to be pointed out that this illustration example is just intended to present the theoretical solutions graphically and to give some possible indications for field applications, other examples could also be easily adopted. The vehicle and bridge properties used in this example are summarized in Table 1. The bridge properties are equivalently calculated based on the original bridge section properties. The initial HL-93 (highway load, developed in 1993) design tandem load is conservatively selected to test the theory and equivalently represented by the theoretical vehicle model. The HL-93 design truckload is not selected due to less reasonable large axle distances. Due to the heavy design tandem load, the vehicle mass is initially calculated as 40% of the total bridge mass. As mentioned earlier, vehicle mass is not limited to the assumption. Although typical vehicles have low frequencies due to the suspension system and inflated tire behaviour for attenuation purposes, the vehicle frequency in this VBI model is initially selected as 300 Hz. The rationale behind this is to avoid the first five bridge frequencies (Table 1) so that the vehicle frequency will not interfere with the extraction of the interested bridge frequencies. Nevertheless, a low vehicle frequency scenario of 5 Hz is also studied in later parameter study section, which shows an

Table 1
Vehicle and bridge parameters used in the analytical baseline study.

Vehicle Property		Bridge Property	
k_v (N·m^{-1})	3.2233 × 10^{11}	EI (N·m^2)	5.0695 × 10^{10}
m_v (kg)	2.268 × 10^4 (40%m_b)	$\bar{m}$ (kg·m^{-1})	1.8779 × 10^3
ξ_v	0.2	ξ_b	0.05
v (m·s^{-1})	8.94	L (m)	30.48
f_v (Hz)	300	f_b (1st - 5th) (Hz)	8.78, 35.14, 79.06, 140.56, 219.62

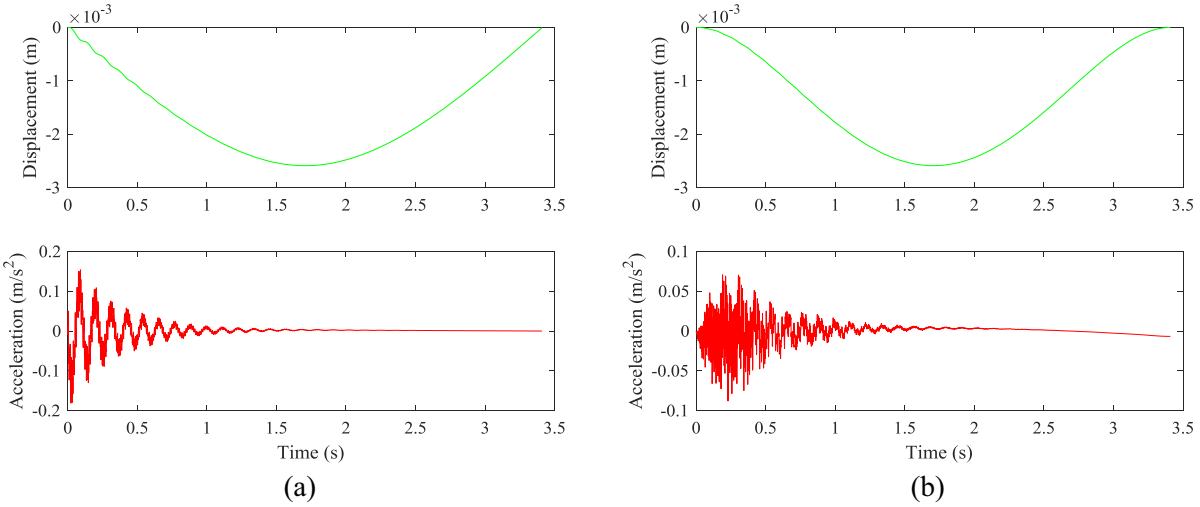

Fig. 2. Displacement and acceleration response of baseline parameters (a) signals from the bridge middle point; (b) signals from the vehicle.

unexpected result and may explain the difficulties of vehicle-based bridge monitoring approach in various experiments. The vehicle stiffness is then calculated based on mass and frequency. The vehicle speed is initially chosen as 20 mph (8.94 m·s^{-1}).

Note that since the bridge has different damping ratios for different vibration modes, as indicated by Eq. (11), the first damping ratio is assumed for the first mode, then unit-length damping constant $\bar{c}$ is calculated based on Eq. (11) before other damping ratios being calculated accordingly. The time step is chosen as 1 × 10^{-3} s, which results in a maximum frequency identification of 500 Hz. To evaluate the frequency identification result, the frequencies of the bridge are obtained by three different approaches: well-established theoretical values (Table 1) based on Eq. (8), the signal from the bridge, and the signal from the vehicle. Specifically, the vehicle acceleration signal is processed by Fast Fourier Transform (FFT) to obtain the bridge frequency information, which is evaluated and compared to the frequency information that is obtained from well-established theory, and the FFT-processed bridge acceleration signal.

The displacement and acceleration responses of the bridge middle point and the vehicle are shown in Fig. 2(a) and (b), respectively. The damping effect can be seen on both the vehicle and the bridge acceleration response not only on the decay phenomenon but also on the signal magnitude, as compared to Fig. 3, in which the damping ratios for both the vehicle and bridge are zeros. The acceleration magnitude from the vehicle with the damping effect is 0.0879 m·s^{-2} (0.9%g), while that of the vehicle without damping scenario is 0.4324 m·s^{-2} (4.4%g). It can be seen here that the inclusion of damping will reduce the signal magnitude as expected, and the decoupling assumption of the equation group is more reasonable if the damping is considered.

The signals from the bridge and the vehicle with damping effects are processed by FFT to obtain the frequency information, as shown in Fig. 4. Note that while the bridge middle point signal is collected for maximum magnitude purpose, the signal at the location of 45% of the total bridge length is collected for the FFT analysis purpose (affected bridge frequency: 20th), as the collected signal may not properly reflect comprehensive bridge frequency information (five frequencies in this case) if the location is not chosen properly. A camel hump phenomenon (both left and right bridge frequency shift) can be observed on the higher bridge vibration modes ($\geq 4^{th}$ in this example) when identifying frequency from the FFT result of the signal from the vehicle, as shown in Fig. 4(b). The camel hump phenomenon is due to the term $\bar{\omega}_{n\pm} = \frac{n\pi v}{L} \pm (\sqrt{1-\xi_n^2})\omega_n$, and can be noticed more clearly when the vehicle has a high speed, as shown in later vehicle speed parameter study Section 5.2. The $\bar{\omega}_{n\pm}$ term also indicates that both high vehicle speed and high frequency mode will have more evident camel hump phenomenon. Table 2 summarizes of the frequency analysis results, note that due to the camel hump phenomenon, the frequencies extracted from vehicle signal are read at the trough of each camel hump. The result is almost the

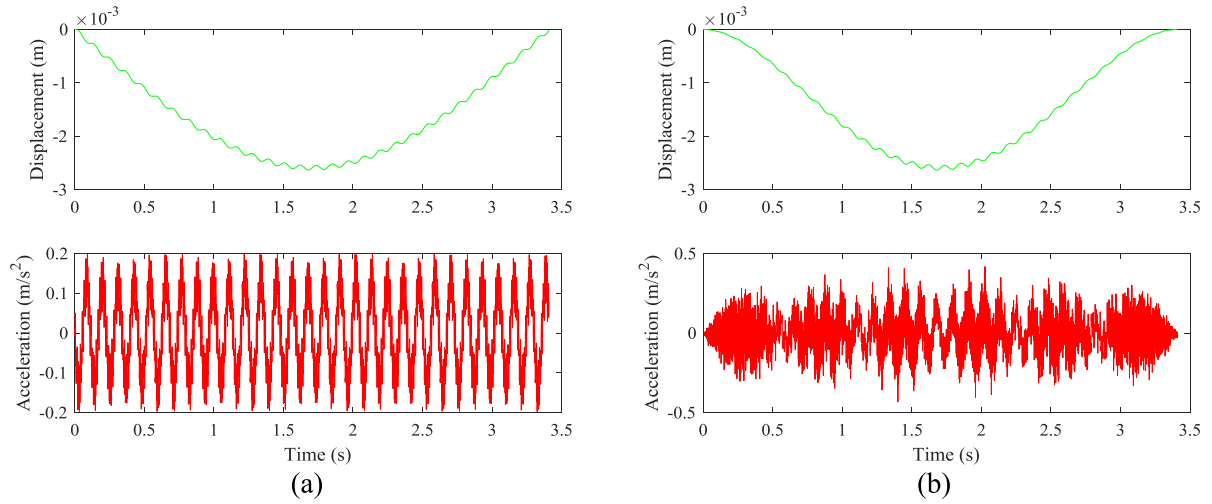

Fig. 3. Displacement and acceleration response with no damping effect ($\xi_v = 0,\ \xi_n = 0$) (a) signals from the bridge middle point; (b) signals from the vehicle.

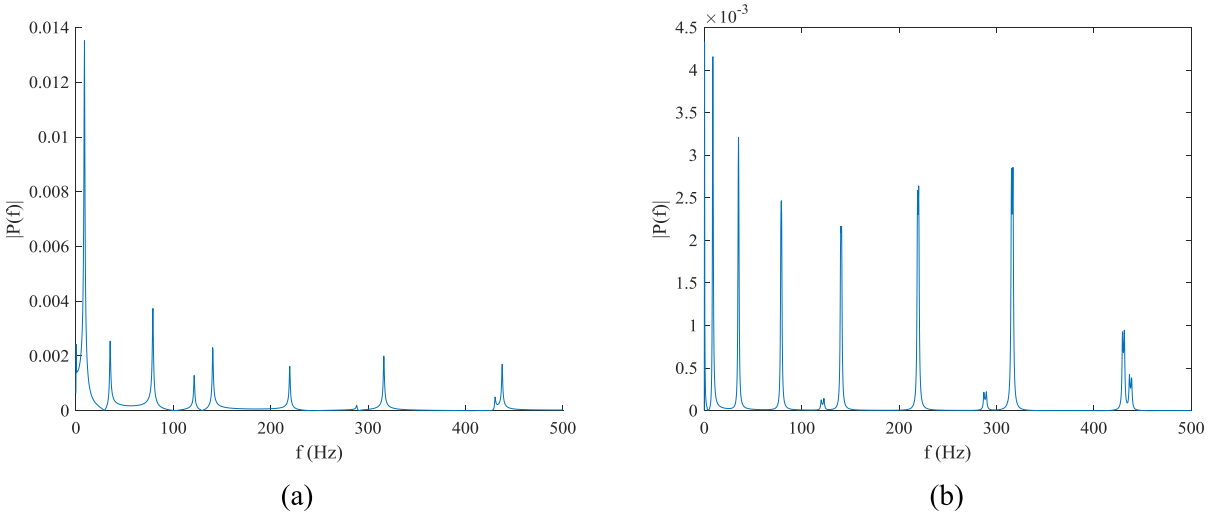

Fig. 4. Frequency analysis results of baseline parameters (a) acceleration signal from the bridge; (b) acceleration signal from the vehicle.

Table 2
Frequency summary of baseline parameters.

Theoretical frequency (Hz)	Signal from bridge		Signal from vehicle	
	Frequency (Hz)	Error (%)	Frequency (Hz)	Error (%)
8.78	8.8	0.23%	8.8	0.23%
35.14	35.19	0.14%	35.19	0.14%
79.06	79.18	0.15%	79.18	0.15%
140.56	140.5	0.04%	140.5	0.04%
219.62	219.6	0.01%	219.6	0.01%

Note: m_v=40% m_b, ξ_b= 0.05, ξ_v= 0.2, f_v= 300 Hz, v= 8.94 m·s^{-1}

same for the signals from the bridge itself and the vehicle, with an excellent error of less than 0.3% from the theoretical values. The next sections will present some parameter effects on extracting multiple bridge frequencies.

4. Bridge damping effect

This section presents the bridge damping effect based on the baseline values in Section 3. Although the damping ratio for real civil structures is usually in the range of 0.02 to 0.1, to cover other types of non-civil structures or devices that may have

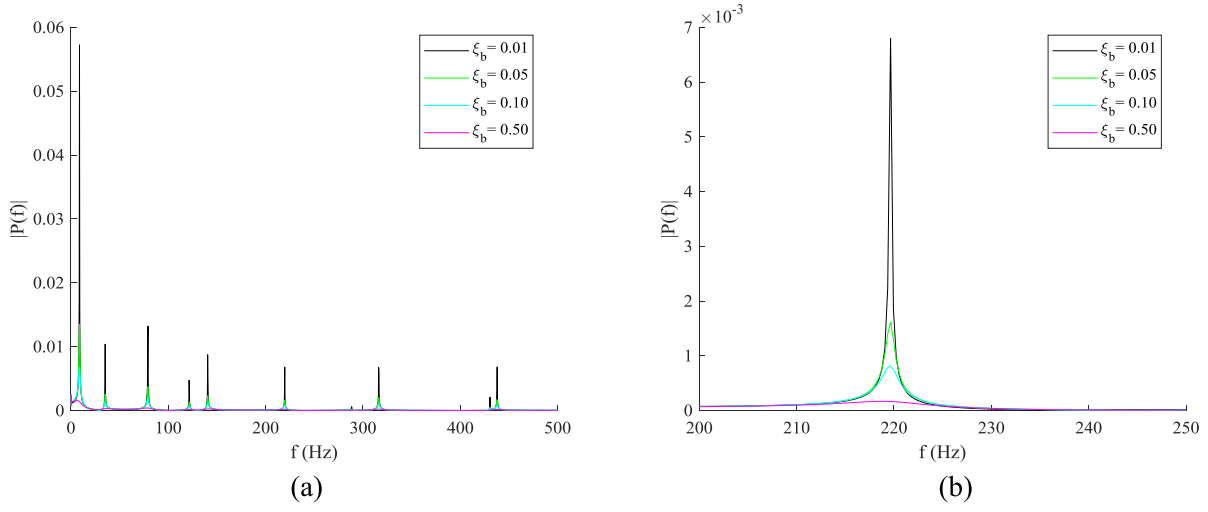

Fig. 5. Frequency analysis of bridge damping effect (signal from the bridge) (a) frequency range of 0-500 Hz; (b) frequency range of 200-250 Hz.

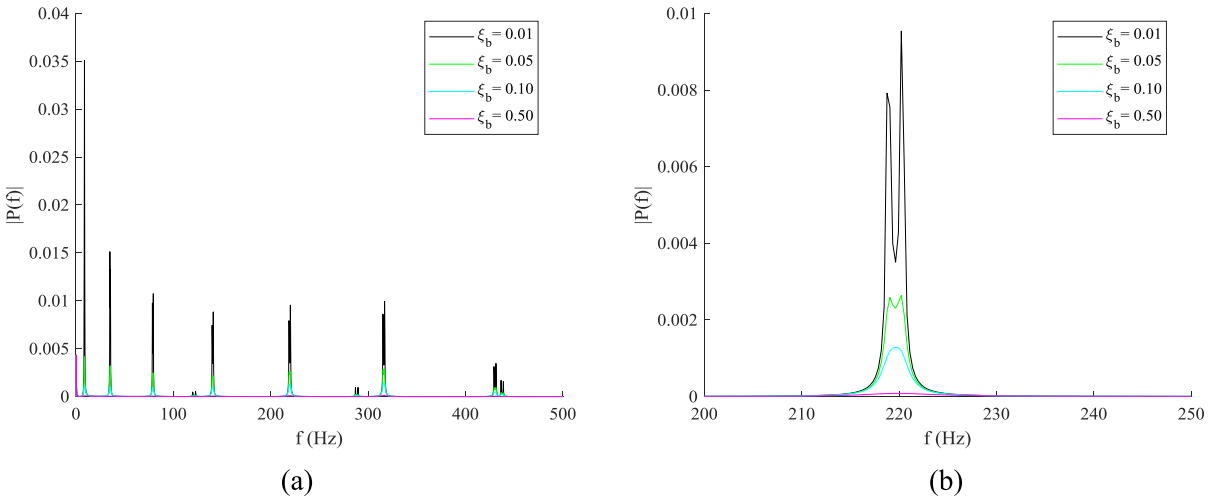

Fig. 6. Frequency analysis of bridge damping effect (signal from the vehicle) (a) frequency range of 0-500 Hz; (b) frequency range of 200-250 Hz.

Table 3
Frequency summary of bridge damping effect (worst scenario).

Theoretical frequency (Hz)	Signal from bridge		Signal from vehicle	
	Frequency (Hz)	Error (%)	Frequency (Hz)	Error (%)
8.78	5.87	33.14%	9.38	6.83%
35.14	35.78	1.82%	36.95	5.15%
79.06	78.89	0.22%	79.77	0.90%
140.56	140.8	0.17%	141.1	0.38%
219.62	219.9	0.13%	219.9	0.13%

Note: m_v=40%m_b, ξ_b= 0.5, ξ_v= 0.2, f_v= 300 Hz, v= 8.94 m·s^{-1}

extreme damping ratios, four different bridge damping ratios (0.01, 0.05, 0.1 and 0.5) are selected to study the effect, while all the other parameters are maintained as the baseline values. Since Section 3 shows that the maximum vehicle acceleration magnitude is 4.4%g for zero bridge and vehicle damping ratios and increasing of damping ratio will only decrease the signal magnitude, the theoretical assumption will only be more reasonable.

Figs. 5 and 6 show the bridge damping effect on the frequency extraction results from the bridge signal (location at 0.45L) and the vehicle, respectively. A specific bridge frequency (5^{th}) is also focused to give a better view. The results show that increasing of bridge damping will lower the magnitude of power spectrum density, which may make it more difficult for the bridge frequencies to be identified, especially for extreme high damping scenario such as 0.5. As shown in Table 3

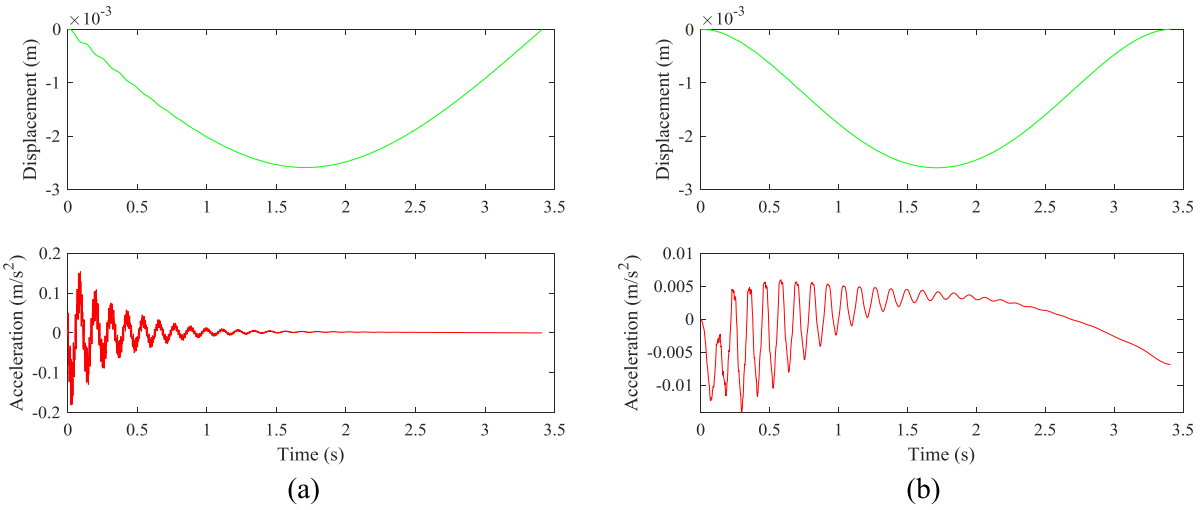

Fig. 7. Displacement and acceleration response due to vehicle frequency effect (f_v=5Hz) (a) signals from the bridge middle point; (b) signals from the vehicle.

Table 4
Frequency summary of vehicle frequency effect (worst scenario).

Theoretical frequency (Hz)	Signal from bridge		Signal from vehicle	
	Frequency (Hz)	Error (%)	Frequency (Hz)	Error (%)
8.78	8.8	0.23%	8.8	0.23%
35.14	35.19	0.14%	35.19	0.14%
79.06	79.18	0.15%	79.18	0.15%
140.56	140.5	0.04%	141.1	0.38%
219.62	219.6	0.01%	220.2	0.26%

Note: m_v=40% m_b, ξ_b= 0.05, ξ_v= 0.2, f_v= 5 Hz, v= 8.94 m·s^{-1}

for the worst bridge damping scenario, the maximum frequency identification errors could be as high as 33.14% and 6.83% for the bridge signal and vehicle signal, respectively. Fig. 6 clearly shows that a camel hump phenomenon can be noticed if the signal is collected from the vehicle, which is also affected by the bridge damping property. Higher bridge damping attenuates the camel hump phenomenon and the magnitude of the power spectrum density of FFT analysis.

5. Vehicle parameter effect

This section presents the effect of several vehicle parameters including frequency, speed, mass and damping on multiple bridge frequencies identification from the vehicle acceleration signal. Each parameter effect is studied while all the other parameters remained as their baseline values in Section 3. The vehicle frequency plays a significant role in attenuating higher bridge frequencies and is preferred to be beyond the interested bridge frequencies. Higher vehicle speed intensifies the vehicle signal magnitude and camel hump phenomenon. Although there is no limitation on the vehicle mass in this theoretical model, it affects the vehicle signal magnitude. A balance should be given among vehicle damping, vehicle speed, and vehicle mass to lower the vehicle acceleration magnitude. Vehicle damping has little effect on extracting multiple bridge frequencies information. Detailed results and discussions of each parameter are presented in the following sections. Note that FFT analysis will be focused on the vehicle signal rather than the bridge signal, although the responses of both will be given for extreme cases.

5.1. Vehicle frequency effect

This section demonstrates that the vehicle frequency plays a significant role in extracting multiple bridge frequencies. Several vehicle frequencies (5Hz, 50Hz, 150Hz, and 300Hz) are selected to study the effect. Fig. 7 shows the responses of the bridge at its middle point and the vehicle for the lowest vehicle frequency (5Hz). The vehicle shows a quite different acceleration response compared to all the other scenarios due to its low frequency. The FFT analysis of the vehicle acceleration signal is shown in Fig. 8, in which the 5th bridge frequency is focused to give a better view. Although the bridge frequency identification error (worst scenario, summarized in Table 4) is low and similar to the baseline result, the feasibility of extracting multiple bridge frequencies from the vehicle may be an issue due to the attenuation effect. The result in Fig. 8 shows that the vehicle frequency has a clear attenuation effect on transmitting the bridge frequencies. The power

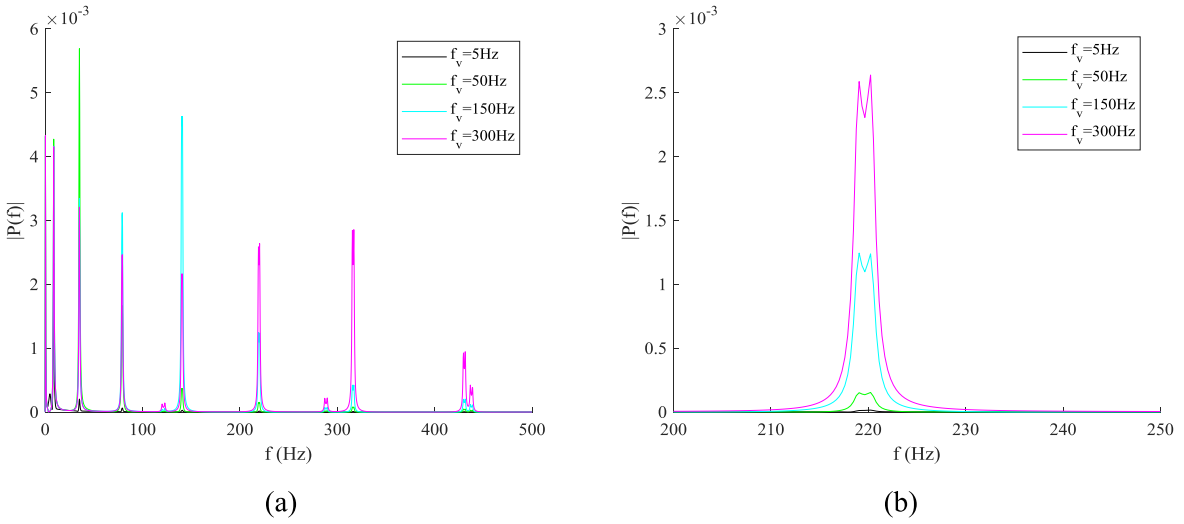

Fig. 8. FFT analysis for studying vehicle frequency effect (a) frequency range of 0-500 Hz; (b) frequency range of 200-250 Hz.

spectral density (PSD) drops to 0.7% and 55.5% from the 1st mode to the 5th mode for the vehicle frequency of 5Hz and 300Hz, respectively. The indication here is that multiple bridge frequencies may be more easily identified if the test vehicle is designed with a high frequency beyond the interested bridge frequency range to be extracted.

The findings of the vehicle frequency effect study in this section are also consistent with experimental observations in the literature. In a field experimental study by Lin and Yang [8], an instrumented cart with a frequency of 1.814 Hz could not identify the second vertical bridge frequency of 14.928 Hz with the lowest vehicle speed, although the first vertical bridge frequency of 3.76 Hz was identified. A realistic heavy truck interacting with a continuous steel girder bridge study by Kim and Lynch [26] in 2012 shows that none of the first four bridge frequencies could be identified from the truck, since the first four bridge frequencies were in the range of 2.25 to 4 Hz, while the identified frequencies of the first and third truck axle were in the range of 10 to 16 Hz, and 8 to 12 Hz, respectively. Besides the truck suspension attenuation effect, the reason could also be the inflated tire effect. Wheel effect studies by Yang et al. [12] also shows that the thin PU (polyurethane) layer coated solid metal wheels performed the best for extracting bridge frequencies compared to the common commercial inflatable wheels and solid rubber wheels. Their ground dynamic tests show that the inflatable wheels and solid rubber wheels had a primary frequency of about 13 Hz and 32 Hz, respectively, while the PU wheels showed no identifiable natural frequencies which may disturb the bridge frequencies. Experimental studies by Urushadze and Yau [16] using a stiffness-adjustable vehicle travelling on a plexiglass beam also shows that vehicle with harder spring gave better identifications of the bridge frequencies. Experimental observations and the theoretical study here indicate that to extract multiple bridge frequencies, attenuation effect from the suspension system and inflated tire may need to be considered, and the test vehicle may need to be specially designed.

5.2. Vehicle speed effect

This section presents the vehicle speed effect with a sequential of vehicle speeds as 20 mph (8.94 $m{\cdot}s^{-1}$), 40 mph (17.88 $m{\cdot}s^{-1}$), 60 mph (26.82 $m{\cdot}s^{-1}$), and 80 mph (35.76 $m{\cdot}s^{-1}$). Fig. 9 shows the responses of the bridge middle point and the vehicle for the highest vehicle speed (35.76 $m{\cdot}s^{-1}$), in which the generated signal length is shortened as approximately 0.85 s. The vehicle speed is also noticed to affect the vehicle signal magnitude, as shown in Fig. 9(b), the magnitude is increased to 0.6001 $m{\cdot}s^{-2}$ (6.12%g). The frequencies are identified as the trough point of each camel hump and are summarized in Table 5. Due to extreme high vehicle speed, the errors of the frequency identification from the bridge and vehicle are increased to 6.49% and 6.83%, respectively. The camel hump phenomenon can be observed on the FFT analysis of the signal from the vehicle, as shown in Fig. 10. Higher vehicle speed and higher bridge vibration mode intensify the camel hump phenomenon, which may adversely affect multiple bridge frequencies identification in field application, as field bridges often involve noise caused by many other factors such as ambient vibration, traffic, and road surface roughness. Higher vehicle speed also shows more attenuation effect, as the PSD drops to 55.5% and 11.1% from the 1st mode to the 5th mode for the vehicle speed of 8.94 $m{\cdot}s^{-1}$ and 35.76 $m{\cdot}s^{-1}$, respectively.

The finding here that the vehicle speed affects the vehicle signal magnitude, is also consistent with the literature, in Yang's experimental study [12], as the speed of the vehicle increases from 2 $km{\bullet}h^{-1}$ to 4 $km{\bullet}h^{-1}$ and then 8 $km{\bullet}h^{-1}$, the acceleration magnitude increases roughly from 50 gals to 100 gals and then 200 gals. Their FFT frequency study also shows that the bridge frequencies are getting more ambiguous as the vehicle speed increases. The explanation could be that the vehicle acceleration magnitude is not negligible compared to g, as 200 gals (2 $m{\cdot}s^{-2}$), is already 20.4%g. The indication here

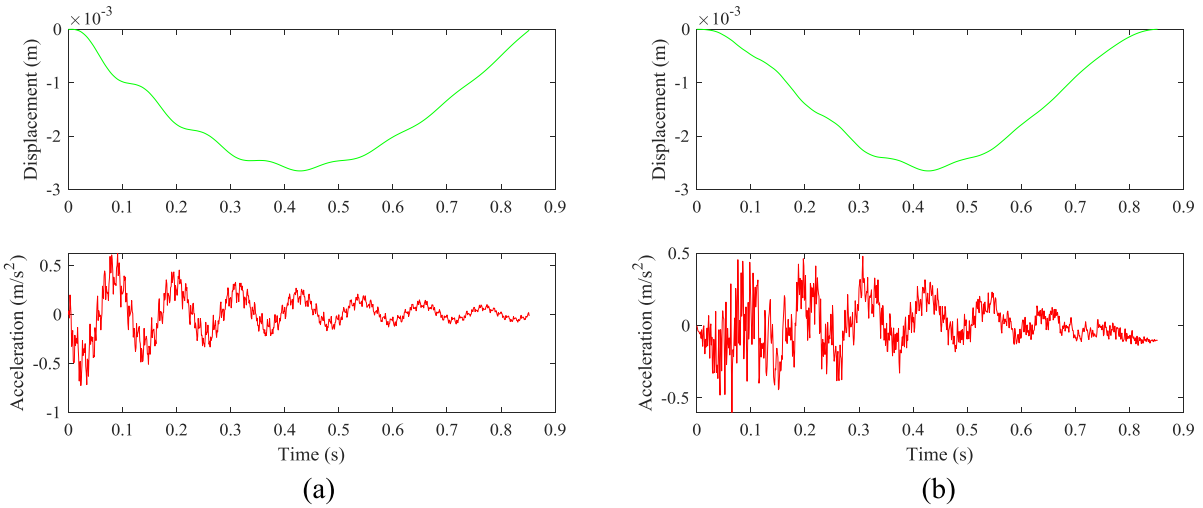

Fig. 9. Displacement and acceleration response due to vehicle speed effect (v=35.76 m·s^{-1}) (a) signals from the bridge middle point; (b) signals from the vehicle.

Table 5
Frequency summary of vehicle speed effect (worst scenario).

Theoretical frequency (Hz)	Signal from bridge		Signal from vehicle	
	Frequency (Hz)	Error (%)	Frequency (Hz)	Error (%)
8.78	8.21	6.49%	9.38	6.83%
35.14	35.17	0.09%	35.17	0.09%
79.06	78.55	0.65%	78.55	0.65%
140.56	140.5	0.04%	140.7	0.10%
219.62	219.2	0.19%	219.2	0.19%

Note: m_v=40% m_b, ξ_b= 0.05, ξ_v= 0.2, f_v= 300 Hz, v= 35.76 m·s^{-1}

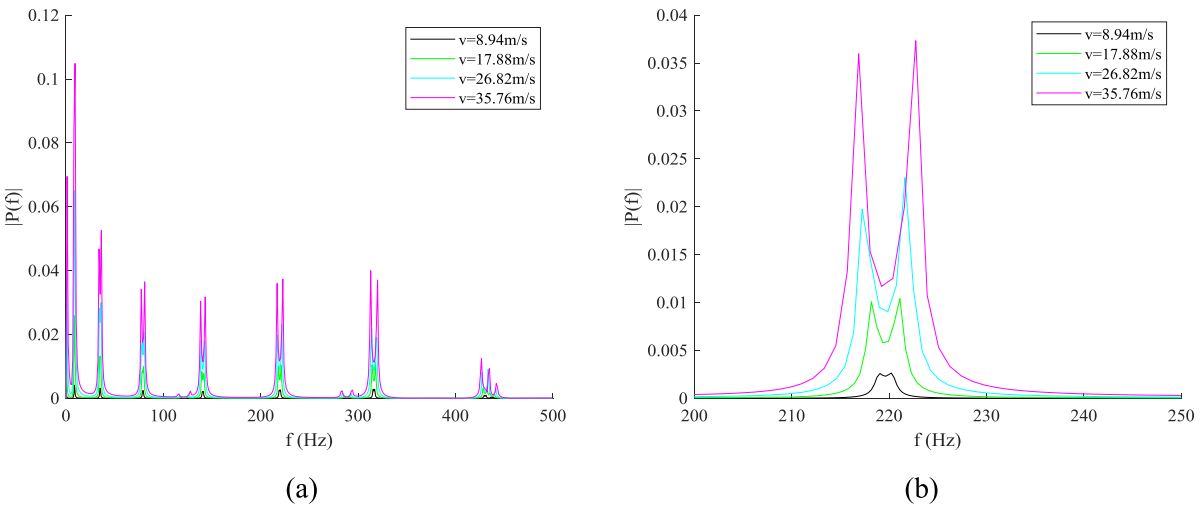

Fig. 10. FFT analysis for studying vehicle speed effect (a) frequency range 0-500 Hz; (b) frequency range 200-250 Hz.

is that to extract multiple bridge frequencies, the vehicle acceleration magnitude may need to be kept far lower than the gravitational acceleration constant.

5.3. Vehicle mass effect

The vehicle mass effect is presented in this section with a sequential vehicle masses of 1%, 10%, 50%, and 100% of the total bridge mass. The vehicle mass affects the vehicle acceleration magnitude which relates to the assumption. Fig. 11 shows the

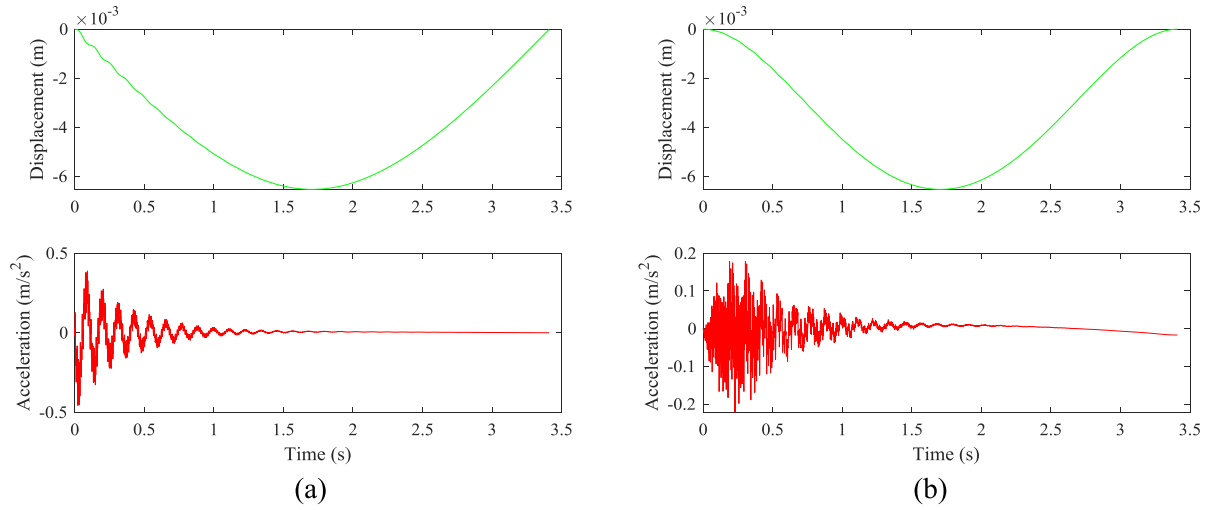

Fig. 11. Displacement and acceleration response due to vehicle mass effect (vehicle mass is 100% of the total bridge mass) (a) signals from the bridge middle point; (b) signals from the vehicle.

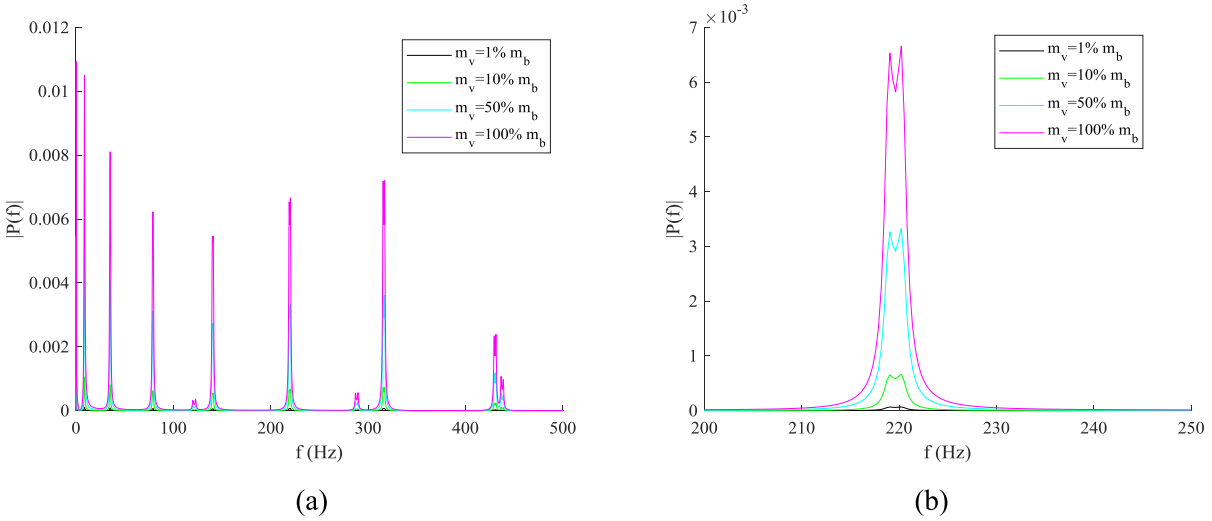

Fig. 12. Frequency analysis for studying vehicle mass effect (a) frequency range 0-500 Hz; (b) frequency range 200-250 Hz.

responses of the bridge middle point and the vehicle for the extreme high vehicle mass scenario. The acceleration magnitude from the vehicle is 0.2219 m·s^{-2} (2.26%g). This result shows that the decoupling assumption may still be reasonable for vehicle mass that is as high as 100% of the total bridge mass if the vehicle is maintained at a low speed. Fig. 12 shows the FFT analysis of the signal from the vehicle for the maximum mass scenario. The vehicle mass parameter shows no attenuation effect, as the PSD drops to 55.5% from the 1st mode to the 5th mode for both the vehicle mass of 1% and 100% of the total bridge mass. Frequency identification result shows the maximum error is as low as the baseline result, as summarized in Table 6.

It may be necessary to mention here that the vehicle mass, vehicle speed, as well as both the vehicle and bridge damping will affect the vehicle acceleration magnitude, which may challenge the theoretical assumption. In a maximum vehicle signal magnitude study in which both the vehicle and bridge damping are ignored, the vehicle is set with a maximum speed (35.76 m·s^{-1}) and maximum mass (100% of the total bridge mass), the vehicle acceleration magnitude is 3.538 m·s^{-2} (36.08%g) and may void the theoretical assumption. Therefore, there is a balance among those parameters to meet the theoretical assumption in this study.

5.4. Vehicle damping effect

This section presents the vehicle damping effect with a sequential of vehicle damping ratios as 0.01, 0.05, 0.1, and 0.5. Fig. 13 show the responses of the bridge middle point and the vehicle for the maximum vehicle damping ratio of 0.5. Due to

Table 6
Frequency summary of vehicle mass effect (worst scenario).

Theoretical frequency (Hz)	Signal from bridge		Signal from vehicle	
	Frequency (Hz)	Error (%)	Frequency (Hz)	Error (%)
8.78	8.8	0.23%	8.8	0.23%
35.14	35.19	0.14%	35.19	0.14%
79.06	79.18	0.15%	79.18	0.15%
140.56	140.5	0.04%	140.5	0.04%
219.62	219.6	0.01%	219.6	0.01%

Note: m_v=100% m_b, ξ_b= 0.05, ξ_v= 0.2, f_v= 300 Hz, v= 8.94 m·s^{-1}

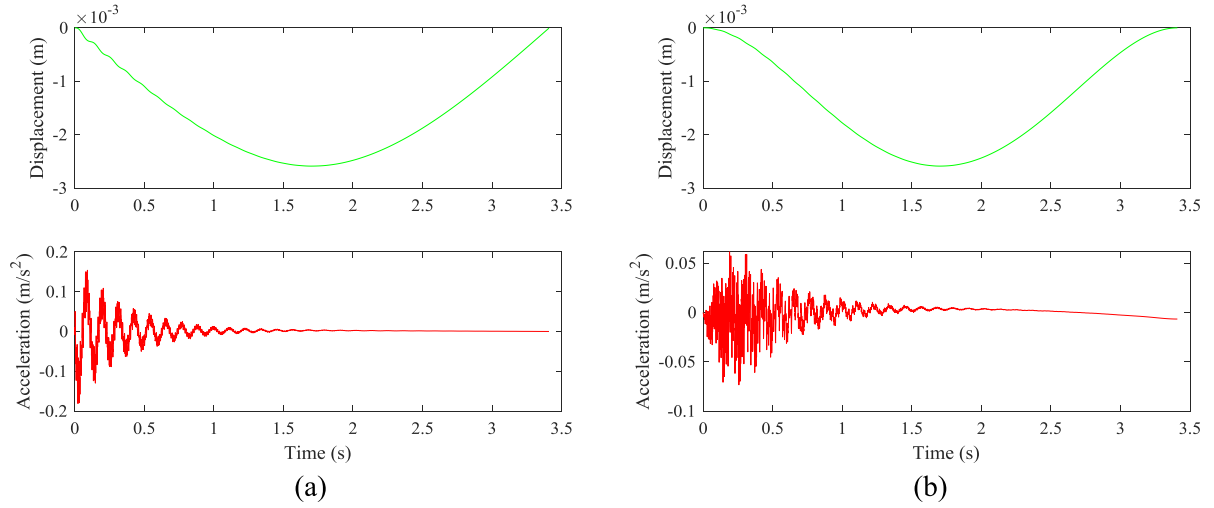

Fig. 13. Displacement and acceleration response due to vehicle damping effect (a) signals from the bridge middle point; (b) signals from the vehicle.

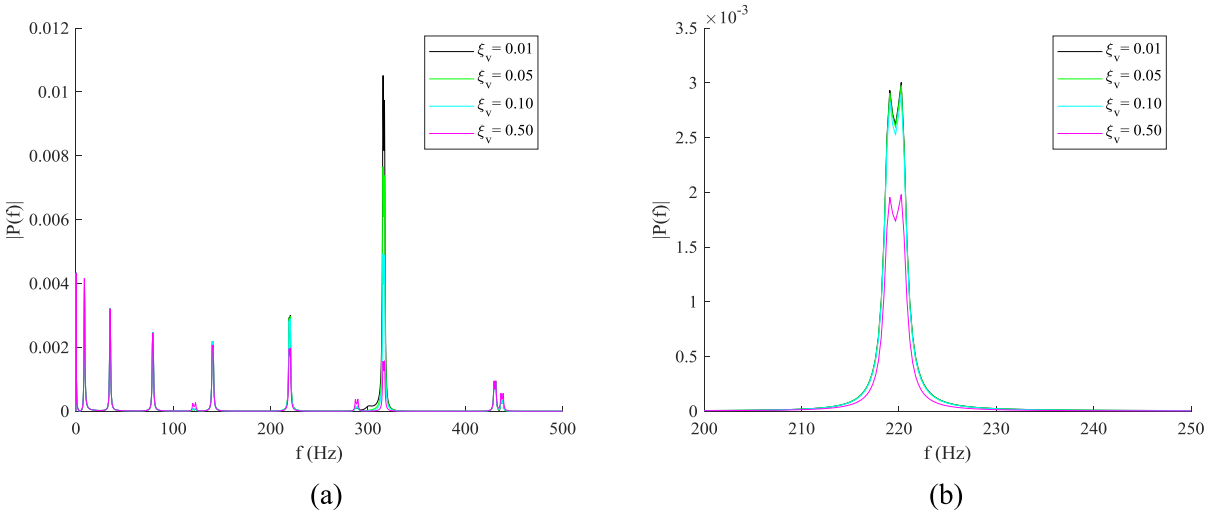

Fig. 14. FFT analysis for studying vehicle damping effect (a) frequency range 0-500 Hz; (b) frequency range 200-250 Hz.

extreme high vehicle damping effect, the acceleration magnitude from the vehicle is decreased from the baseline of 0.0879 m·s^{-2} (0.9%g) to 0.0734 m·s^{-2} (0.75%g). Fig. 14 shows the FFT analysis of the vehicle acceleration signals for different vehicle damping ratios, and Table 7 summarizes the FFT results for the extreme high vehicle damping scenario, both of them show that the vehicle damping has little effect on extracting multiple bridge frequencies from the vehicle. The vehicle damping parameter shows some attenuation effect, since the PSD drops to 62.9% and 41.8% from the 1st mode to the 5th mode for the vehicle damping ratio of 0.01 and 0.5, respectively.

Table 7
Frequency summary of vehicle damping effect (worst scenario).

Theoretical frequency (Hz)	Signal from bridge		Signal from vehicle	
	Frequency (Hz)	Error (%)	Frequency (Hz)	Error (%)
8.78	8.8	0.23%	8.8	0.23%
35.14	35.19	0.14%	35.19	0.14%
79.06	79.18	0.15%	79.18	0.15%
140.56	140.5	0.04%	140.5	0.04%
219.62	219.6	0.01%	219.6	0.01%

Note: m_v=40%m_b, ξ_b= 0.05, ξ_v= 0.5, f_v= 300 Hz, v= 8.94 m·s^{-1}

6. Conclusions

The general coupled differential equation group for the vehicle bridge interaction model without bridge boundary restriction is reestablished to include both the vehicle and bridge damping effect, and important parameters that affect multiple bridge frequencies extraction from the vehicle are studied based on the simply supported boundary condition scenario. New theoretical simplification assumption requires that the vehicle acceleration magnitude should be much lower than the gravitational acceleration constant so that the equation group could be uncoupled, and theoretical solutions could be obtained. This assumption requires a balance among all the parameters including the bridge condition, vehicle mass, speed, and damping. This theoretical work may give some indications for designing a special field test vehicle to monitor bridge in a more comprehensive way. Several conclusions can be drawn regarding the parameter studies include:

1) Damping coefficient certainly affects both the vehicle and bridge vibration behaviour. However, structures with extreme high damping would adversely affect its dynamic properties transmission to the test vehicle, while the vehicle damping has little effect when extracting multiple bridge frequencies. The vehicle damping parameter also shows increasing attenuation effect, as the power spectral density drops to 62.9% and 41.8% from the 1st mode to the 5th mode for the vehicle damping ratio of 0.01 and 0.5, respectively.
2) The vehicle frequency parameter shows significant attenuation effect on the bridge frequencies compared to all the other parameters. The power spectral density drops to 0.7% and 55.5% from the 1st mode to the 5th mode for the vehicle frequency of 5Hz and 300Hz, respectively. Therefore vehicle frequency is preferred to be designed beyond the interested bridge frequencies to be extracted. For field application, the inflated tires and suspension system of the test vehicle may need to be addressed to better reflect the vibration behaviour of the bridge.
3) Higher vehicle speed not only increases the vehicle acceleration magnitude and challenges the assumption, but also intensifies the camel hump phenomenon, which may adversely disturb multiple bridge frequencies identification during experiments. Higher vehicle speed also shows more attenuation effect, as the power spectral density drops to 55.5% and 11.1% from the 1st mode to the 5th mode for the vehicle speed of 8.94 m·s^{-1} and 35.76 m·s^{-1}, respectively.
4) Although vehicle mass is not limited in this theoretical model, it affects the theoretical assumption along with other parameters. Vehicle mass parameter may need to be balanced with vehicle speed and damping parameters to meet the theoretical assumption. The vehicle mass parameter shows no attenuation effect on the frequency analysis.

Declaration of Competing Interest

The authors declare that they have no known competing financial interests or personal relationships that could have appeared to influence the work reported in this paper.

CRediT authorship contribution statement

Zhenhua Shi: Conceptualization, Methodology, Software, Validation, Formal analysis, Investigation, Resources, Data curation, Writing - original draft, Writing - review & editing, Visualization. **Nasim Uddin:** Conceptualization, Resources, Writing - review & editing, Supervision, Project administration, Funding acquisition.

Acknowledgement

The authors would like to express their gratitude to the financial support received from the National Science Foundation [grant numbers: NSF-CNS-1645863, NSF-CSR-1813949]. The authors also appreciate the comments and feedback received from Prof. E.J. OBrien.

Supplementary materials

Supplementary material associated with this article can be found, in the online version, at doi:10.1016/j.jsv.2020.115735.

References

[1] A. Žnidaric, Bridge weigh-in-Motion, Int. Conf. Heavy Veh. HV Paris 2008 (2013) 269–269, doi:10.1002/9781118623305.part4.
[2] D. Cantero, A. González, Bridge damage detection using weigh-in-motion technology, J. Bridge Eng. 20 (5) (2015) 04014078, doi:10.1061/(asce)be.1943-5592.0000674.
[3] Y. Yu, Cai C, L. Deng, State-of-the-art review on bridge weigh-in-motion technology, Adv. Struct. Eng. 19 (9) (2016) 1514–1530, doi:10.1177/1369433216655922.
[4] E.J. OBrien, P.C. Fitzgerald, A. Malekjafarian, E. Sevillano, Bridge damage detection using vehicle axle-force information, Eng. Struct. 153 (2017) 71–80, doi:10.1016/j.engstruct.2017.10.012.
[5] A. Malekjafarian, P.J. McGetrick, E.J. OBrien, A review of indirect bridge monitoring using passing vehicles, Shock Vib. (2015), doi:10.1155/2015/286139.
[6] Y.B. Yang, J.P. Yang, State-of-the-art review on modal identification and damage detection of bridges by moving test vehicles, Int. J. Struct. Stab. Dy. 18 (02) (2018) 1850025, doi:10.1142/s0219455418500256.
[7] Y.B. Yang, C.W. Lin, J.D. Yau, Extracting bridge frequencies from the dynamic response of a passing vehicle, J. Sound Vib. (2004) 471–493, doi:10.1016/s0022-460x(03)00378-x.
[8] C.W. Lin, Y.B. Yang, Use of a passing vehicle to scan the fundamental bridge frequencies: an experimental verification, Eng. Struct. 27 (13) (2005) 1865–1878, doi:10.1016/j.engstruct.2005.06.016.
[9] P.J. McGetrick, A. Gonzlez, E.J. OBrien, Theoretical investigation of the use of a moving vehicle to identify bridge dynamic parameters, Insight-Non-Destruct. Test. Cond. Monitor. 51 (8) (2009) 433–438, doi:10.1784/insi.2009.51.8.433.
[10] Y.B. Yang, K.C. Chang, Extraction of bridge frequencies from the dynamic response of a passing vehicle enhanced by the EMD technique, J. Sound Vib. (2009) 718–739, doi:10.1016/j.jsv.2008.11.028.
[11] Y.B. Yang, K.C. Chang, Extracting the bridge frequencies indirectly from a passing vehicle: parametric study, Eng. Struct. 31 (10) (2009) 2448–2459, doi:10.1016/j.engstruct.2009.06.001.
[12] Y.B. Yang, W.F. Chen, H.W. Yu, C.S. Chan, Experimental study of a hand-drawn cart for measuring the bridge, Eng. Struct. (2013) 222–231, doi:10.1016/j.engstruct.2013.09.007.
[13] J.P. Yang, W.C. Lee, Damping effect of a passing vehicle for indirectly measuring bridge frequencies by EMD technique, Int. J. Struct. Stab. Dynam. 18 (01) (2018) 1850008, doi:10.1142/s0219455418500086.
[14] J.P. Yang, C.Y. Cao, Wheel size embedded two-mass vehicle model for scanning bridge frequencies, Acta Mech. 231 (4) (2020) 1461–1475, doi:10.1007/s00707-019-02595-5.
[15] Y.B. Yang, W.F. Chen, Extraction of bridge frequencies from a moving test vehicle by stochastic subspace identification, J. Bridge Eng. 21 (3) (2016) 04015053, doi:10.1061/(asce)be.1943-5592.0000792.
[16] S Urushadze, J.D. Yau, Experimental verification of indirect bridge frequency measurement using a passing vehicle, Procedia Eng. 190 (2017) 554–559, doi:10.1016/j.proeng.2017.05.379.
[17] Y.B. Yang, Y.C. Li, K.C. Chang, Constructing the mode shapes of a bridge from a passing vehicle: a theoretical study, Smart Struct. Syst. 13 (5) (2014) 797–819, doi:10.12989/sss.2014.13.5.797.
[18] A. Malekjafarian, E.J. OBrien, Identification of bridge mode shapes using short time frequency domain decomposition of the responses measured in a passing vehicle, Eng. Struct. 81 (2014) 386–397, doi:10.1016/j.engstruct.2014.10.007.
[19] E.J. OBrien, A. Malekjafarian, A mode shape-based damage detection approach using laser measurement from a vehicle crossing a simply supported bridge, Struct. Control Heallth. 23 (10) (2016) 1273–1286, doi:10.1002/stc.1841.
[20] A. Malekjafarian, E.J. OBrien, On the use of a passing vehicle for the estimation of bridge mode shapes, J. Sound Vib. 397 (2017) 77–91, doi:10.1016/j.jsv.2017.02.051.
[21] Z.Q. Qi, F.T.K. Au, Identifying mode shapes of girder bridges using dynamic responses extracted from a moving vehicle under impact excitation, Int. J. Struct. Stab. Dy. 17 (08) (2017) 1750081, doi:10.1142/s021945541750081x.
[22] Y.B. Yang, B Zhang, Y Qian, Y Wu, Contact-point response for modal identification of bridges by a moving test vehicle, Int. J. Struct. Stab. Dy. (2018) 1850073, doi:10.1142/s0219455418500736.
[23] A. González, E.J. OBrien, P.J. McGetrick, Identification of damping in a bridge using a moving instrumented vehicle, J. Sound Vib. 331 (18) (2012) 4115–4131, doi:10.1016/j.jsv.2012.04.019.
[24] J. Keenahan, E.J. OBrien, P.J. McGetrick, A. Gonzalez, The use of a dynamic truck–trailer drive-by system to monitor bridge damping, Struct. Health Monit. 13 (2) (2014) 143–157, doi:10.1177/1475921713513974.
[25] Y.B. Yang, J.P. Yang, B. Zhang, Y.T. Wu, Vehicle Scanning Method for Bridges, John Wiley and Sons, Ltd., London, 2019, doi:10.1002/9781119539629.
[26] J. Kim, J.P. Lynch, Experimental analysis of vehicle–bridge interaction using a wireless monitoring system and a two-stage system identification technique, Mech. Syst. Signal Pr. 28 (2012) 3–19, doi:10.1016/j.ymssp.2011.12.008.
[27] C.W. Kim, R. Isemoto, P.J. McGetrick, M. Kawatani, E.J. OBrien, Drive-by bridge inspection from three different approaches, Smart Struct. Syst. 13 (5) (2014) 775–796, doi:10.12989/sss.2014.13.5.775.
[28] F. Cerda, S. Chen, J. Bielak, J.H. Garrett, P. Rizzo, J. Kovačević, Indirect structural health monitoring of a simplified laboratory-scale bridge model, Smart Struct. Syst. 13 (5) (2014) 849–868, doi:10.12989/sss.2014.13.5.849.
[29] P.J. McGetrick, C.W. Kim, A. González, E.J. OBrien, Experimental validation of a drive-by stiffness identification method for bridge monitoring, Struct. Health Monit. 14 (4) (2015) 317–331, doi:10.1177/1475921715578314.
[30] C.W. Kim, K.C. Chang, J McGetrick, S. Inoue, S. Hasegawa, Utilizing moving vehicles as sensors for bridge condition screening-a laboratory verification, Sens. Mater 29 (2) (2017) 153–163, doi:10.18494/sam.2017.1433.
[31] MATLAB, Version R2019a (9.6.0.1072779), The MathWorks Inc., Natick, Massachusetts, 2019.
[32] M. Paz, W. Leigh, Structural Dynamics: Theory and Computation, 5th Edition, Springer Science & Business Media, Inc., New York, 2004, doi:10.1007/978-1-4615-0481-8.
[33] R.M. Barker, J.A. Puckett, Design of highway bridges: An LRFD approach [M], John wiley & sons, 2013, doi:10.1002/9781118411124.